PCCP

PAPER

View Article Online
View Journal | View Issue

Published on 13 January 2015. Downloaded by Universidade de Coimbra on 06/02/2015 10:42:20.

Cite this: *Phys. Chem. Chem. Phys.*, 2015, **17**, 5155

A molecular view of cisplatin's mode of action: interplay with DNA bases and acquired resistance†‡

M. Paula M. Marques,*[ab] Diego Gianolio,[c] Giannantonio Cibin,[c] John Tomkinson,[d] Stewart F. Parker,[d] Rosendo Valero,[a] R. Pedro Lopes[a] and Luis A. E. Batista de Carvalho*[a]

Received 9th November 2014,
Accepted 7th January 2015

DOI: 10.1039/c4cp05183a

www.rsc.org/pccp

The interaction of the widely used anticancer drug cisplatin with DNA bases was studied by EXAFS and vibrational spectroscopy (FTIR, Raman and INS), coupled with DFT/plane-wave calculations. Detailed information was obtained on the local atomic structure around the Pt(II) centre, both in the cisplatin–purine (adenine and guanine) and cisplatin–glutathione adducts. Simultaneous neutron and Raman scattering experiments allowed us to obtain a reliable and definite picture of this cisplatin interplay with its main pharmacological target (DNA), at the molecular level. The vibrational experimental spectra were fully assigned in the light of the calculated pattern for the most favoured geometry of each drug–purine adduct, and cisplatin's preference for guanine (G) relative to adenine (A) within the DNA double helix was experimentally verified: a complete N by S substitution in the metal coordination sphere was only observed for [cDDP–A_2], reflecting a somewhat weaker Pt–A binding relative to Pt–G. The role of glutathione on the drug's pharmacokinetics, as well as on the stability of platinated DNA adducts, was evaluated as this is the basis for glutathione-mediated intracellular drug scavenging and *in vivo* resistance to Pt-based anticancer drugs. Spectroscopic evidence of the metal's preference for glutathione's sulfur over purine's nitrogen binding sites was gathered, at least two sulfur atoms being detected in platinum's first coordination sphere.

Introduction

Pt(II) compounds constitute a specific class of DNA-damaging anticancer agents, cisplatin (*cis*-$(NH_3)_2PtCl_2$, cDDP),[1,2] carboplatin and oxaliplatin being currently in clinical use, while numerous other Pt(II) complexes are being developed aiming at an increased antineoplastic activity coupled with a lower toxicity and a decreased acquired resistance.[3–5] The anticancer capacity of this kind of agents is recognized to be due to severe DNA damage through selective covalent binding of Pt(II) to the purine and pyrimidine bases (mainly the purines adenine (A) and guanine (G)).[6–8] These inter- and intrastrand platinum–DNA adducts are formed following drug uptake into the cell nucleus, upon drug hydrolysis (by sequential loss of the chloride ligands and aquation). However, despite the success of cisplatin and new generation platinum-based anticancer agents, acquired resistance is still one of the main limiting factors for their clinical application. In particular, endogenous thiols, such as glutathione (GSH, L-γ-glutamyl-cysteinyl-glycine (Glu-Cys-Gly)), are known to intercept this type of compounds due to the high reactivity of Pt(II) towards S-donor ligands[9–12] that may hinder the metal-agent from even reaching DNA in therapeutically significant amounts. Rational drug design is based on a thorough understanding of the drug's mode of action, as well as of the mechanisms underlying acquired resistance. These, in turn, rely on a detailed knowledge, at the molecular level, of the interactions established by the newly developed agent with its biological target, and with other relevant biomolecules that may affect the drug's pharmacokinetics.

The lack of good quality crystals for this kind of Pt-based adducts, has, to this date, hindered its accurate structural study. In spite of the large number of studies on this subject, including the newly reported resonant inelastic X-ray scattering (RIXS) experiment on cisplatin interaction with DNA in aqueous medium,[13]

[a] *Molecular Physical Chemistry R&D Unit, Fac. Science and Technology, Univ. Coimbra, 3004-535 Coimbra, Portugal. E-mail: pmc@ci.uc.pt, labc@ci.uc.pt; Fax: +351-239-826541; Tel: +351-239-826541*
[b] *Dep. Life Sciences, Fac. Science and Technology, Univ. Coimbra, Portugal*
[c] *Diamond Light Source, STFC Harwell Science and Innovation Campus, Chilton, UK*
[d] *ISIS Facility, STFC Rutherford Appleton Laboratory, Chilton, Didcot, OX 11 0QX, UK*

† Dedicated to Professor José J. C. Teixeira-Dias, FRSC, CSci, on the occasion of his 70th birthday.

‡ Electronic supplementary information (ESI) available. See DOI: 10.1039/c4cp05183a

Published on 13 January 2015. Downloaded by Universidade de Coimbra on 06/02/2015 10:42:20.

the detailed molecular picture of the drug's binding to the DNA bases, particularly the favoured Pt-coordination to the N^7 atom from guanine and adenine, still needs clarification, aiming at the elucidation of the local environment of the drug's metal centre either in the presence of its major target (DNA purine bases) or of potential inactivating biomolecules (*e.g.* GSH). The present study contributes to this goal, by coupling three forms of vibrational spectroscopy (infrared (FTIR), Raman and inelastic neutron scattering (INS)) with computational simulations and extended X-ray absorption fine structure (EXAFS). The latter is a method of choice for obtaining detailed information on the local structure of bioinorganic non-crystalline materials,[14–16] since even the weakest chemical bonds are not affected by the measurement, and is expected to fully elucidate cisplatin's interplay with DNA – its binding mode to adenine and guanine, and the effect of GSH on the drug's bioavailability. Indeed, this technique has been used successfully by other authors[15,16] for the study of the degradation of antitumour Pt(II) complexes in the presence of sulfur nucleophiles.

Inelastic neutron scattering spectroscopy, in turn, is particularly appropriate to study materials containing hydrogen atoms, since the scattering cross section for hydrogen (^{1}H) (about 80 barns) is much larger than for most other elements (at most *ca.* 5 barns). The neutron scattering cross-section of an element (σ) is a characteristic of each isotope and independent of the chemical environment. During the scattering event, a fraction of the incoming neutron energy can be used to cause vibrational excitation, and the vibrational modes with the largest hydrogen displacements will dominate the spectrum. Therefore, INS will be particularly important in solids in which the molecular units are linked together by hydrogen close contacts, such as cisplatin, and the lowest-frequency vibrations are those expected to be most affected.

This study is aimed at achieving a better understanding, at the molecular level, of cisplatin's mode of action, regarding its pharmacodynamics – interplay with DNA – and pharmacokinetics – glutathione-mediated acquired resistance. The drug's adducts with guanine and adenine were investigated, as well as their glutathione counterparts, with a view to: (i) unequivocally determine the local environment of the absorbing Pt(II) centre in these systems, in order to accurately determine their first coordination sphere content, as well as the metal's binding preferences towards these molecules; (ii) obtain experimental proof of the drug's preference for guanine over adenine, which has been suggested to result from the structural difference between the two purine bases, guanine displaying a carbonyl group allowing the formation of a stabilizing H-bond that may favor cDDP–G as compared to cDDP–A; (iii) assess the competition between reduced glutathione (GSH) and purines for cisplatin, since this ubiquitous antioxidant is recognized to be one of the main targets responsible for the *in vivo* inactivation of cisplatin (acquired resistance) and induction of toxicity (*e.g.* nephrotoxicity), due to the expected higher affinity of Pt(II) for glutathione's sulfur over purine's nitrogens.

The data obtained along this study were interpreted on the basis of the extensive theoretical and experimental work available for these systems,[13,17–20] including previous data gathered by the authors (by vibrational spectroscopy and theoretical calculations) for cisplatin and cisplatin-like agents,[21–26] as well as for guanine,[27] adenine[28] and glutathione. The detailed knowledge of the molecular basis of the cDDP–guanine/adenine and cDDP–glutathione interplay gathered in this work will pave the way for future studies on other platinum and palladium-based agents previously characterized by the authors and assessed as to their cytotoxicity towards several human cancer cell lines.[29–37] This will provide valuable clues for the rational design of novel cisplatin-like drugs, displaying a higher efficiency, lower toxicity, decreased acquired resistance and possible oral administration.

Experimental

Chemicals

cis-Diammineplatinum(II) dichloride (Cisplatin, cDDP, $Pt(NH_3)_2Cl_2$, >98%), potassium tetrachloroplatinate(II) (K_2PtCl_4, >99.9%), tetraammineplatinum(II) nitrate ($Pt(NH_3)_4{\cdot}(NO_3)_2$, 99.99%), adenine ($C_5H_5N_5$, >99%), guanine ($C_5H_5N_5O$, 98%), reduced L-glutathione ($H_2NCH(CO_2H)CH_2CH_2CONHCH(CH_2SH)CONHCH_2CO_2H$, >98%) and silver nitrate ($AgNO_3$, >99%) were purchased from Sigma-Aldrich Química S.A. (Sintra, Portugal).

Synthesis

Platinum–glutathione complex. The $Pt(GSH)_4$ complex was prepared from a K_2PtCl_4 solution by adding four molar equivalents of reduced L-glutathione. The final product was obtained in the form of a yellow precipitate after stirring for one hour at room temperature.

Cisplatin–purine adducts. Cisplatin–adenine and cisplatin–guanine adducts were synthesized in 1:1 and 1:2 molar ratios (cDDP–G, cDDP–A, cDDP–G_2 and cDDP–A_2, respectively), following an optimized synthetic route based on reported methods.[38,39]

For cDDP–G_2 a 0.2 mmol dm^{-3} *cis*-$Pt(NH_3)_2Cl_2$ solution was prepared, while for cDDP–A_2 a more concentrated 7.5 mmol dm^{-3} cisplatin solution was used. In an initial step, the hydrolysis of chloride ligands was induced by adding 1.9 molar equivalents of $AgNO_3$ while stirring at 40 °C, in the dark, for approximately one hour. The activated cisplatin solutions were then centrifuged at 16 000 rpm for 10 min, AgCl was removed by filtration, and 1 or 2 molar equivalents of purine base (either A or G) were added to yield 1:1 or 1:2 adducts, respectively. These solutions were stirred for *ca.* 40 hours at 30 °C, in the dark,[40] and then centrifuged and filtered to remove unreacted purine. The pH was adjusted to 3.9 for cDDP–G_2 and at 5.1 for cDDP–A_2. In a final step, the adduct solutions were concentrated by evaporation under vacuum, followed by lyophilisation, and the solid products were stored at room temperature, in the dark.

Cisplatin–glutathione adducts. 1:1 and 1:2 molar equivalents of GSH were added to a 3.0 mmol dm^{-3} cisplatin solution, and stirring was maintained in the dark, at room temperature, for 24 hours. The initial colourless solution became deep yellow over time (a characteristic colour of complexes containing Pt–S

 This journal is © the Owner Societies 2015

Published on 13 January 2015. Downloaded by Universidade de Coimbra on 06/02/2015 10:42:20.

covalent bonds[41]). The cDDP–GSH and cDDP–GSH_2 solutions were then concentrated by evaporation under vacuum, and lyophilized to obtain a yellow powder.

Titration of cisplatin–purine adducts with glutathione. The cDDP–G_2 and cDDP–A_2 adducts were titrated with GSH, by dissolving approximately 0.1 g of each compound in 180 mL of water. Reduced glutathione was added, in a molar ratio of 1 : 1 or 1 : 2 (for a partial or a complete titration, respectively). The reaction mixtures were kept in the dark with stirring, at room temperature for 24 hours, after which they were centrifuged at 16 000 rpm, for 10 minutes, and filtered to remove precipitated adenine or guanine. Finally, they were concentrated under vacuum, at 30 °C and lyophilized to yield the solid (white) products.[42]

Vibrational spectroscopy

FTIR. The FTIR spectra were recorded using a Bruker Optics Vertex 70 FTIR spectrometer, in the 400–4000 cm^{-1} range, in KBr disks (*ca.* 1% (w/w)). A KBr beamsplitter and a liquid nitrogen cooled Mercury Cadmium Telluride (MCT) detector

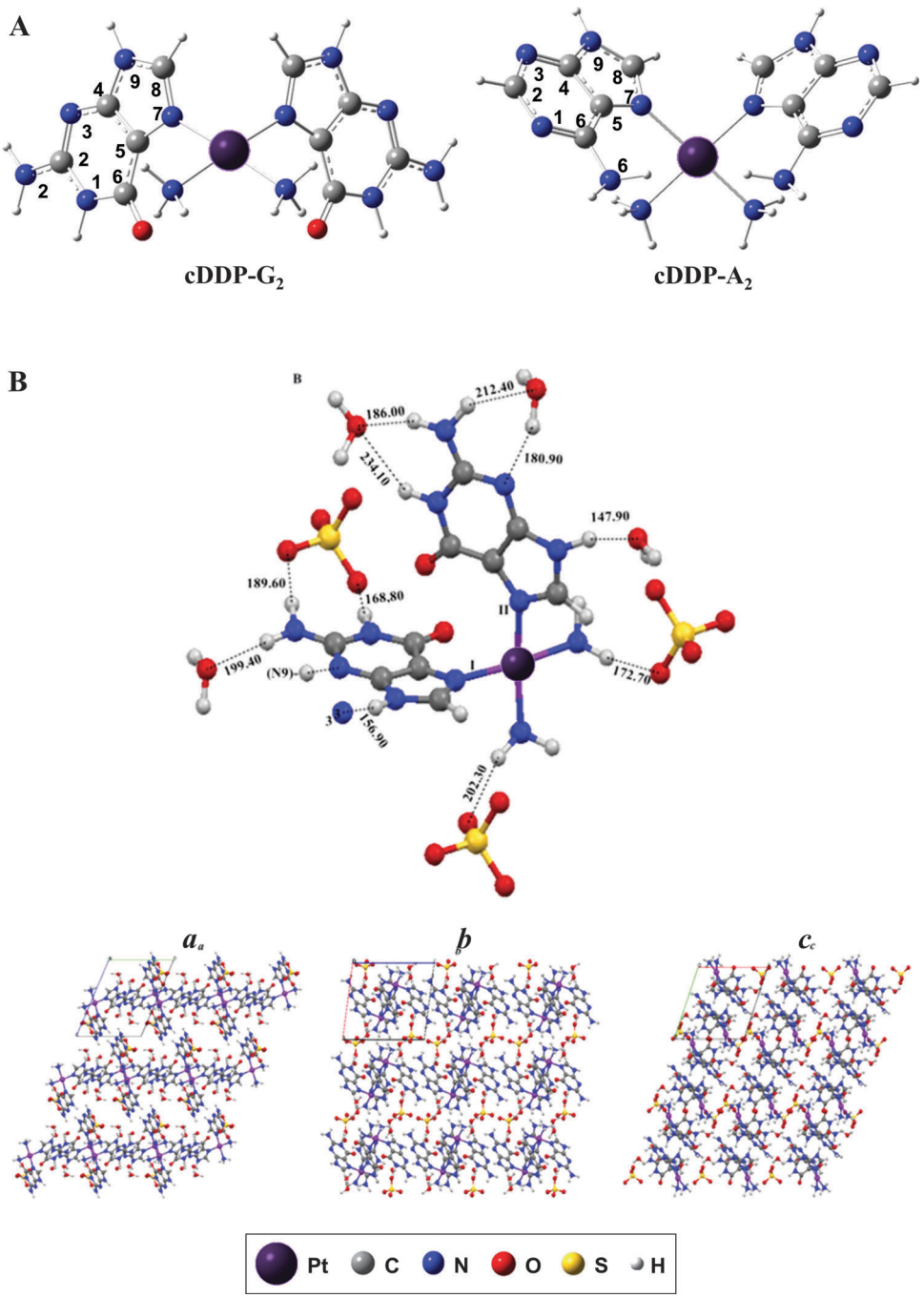

Fig. 1 Calculated structures for the cDDP–G_2 and cDDP–A_2 adducts: (A) isolated molecule (DFT/mPW1PW). (B) Condensed phase for cDDP–G_2 (DFT-PW); the three-dimensional lattice is shown along the *a*, *b* and *c* unit cell vectors (the atom numbering is included).

Published on 13 January 2015. Downloaded by Universidade de Coimbra on 06/02/2015 10:42:20.

were used. The spectra were collected for 2 minutes, with 2 cm^{-1} resolution. The error in wavenumbers was estimated to be less than 1 cm^{-1}.

Raman. The Raman spectra were recorded using a triple monochromator HORIBA Jobin-Yvon T64000 Raman system (focal distance 0.640 m, aperture f/7.5), equipped with holographic gratings of 1800 grooves mm^{-1}. The premonochromator stage was used in the subtractive mode. The detection system was a liquid nitrogen cooled non-intensified 1024 × 256 pixel (1″) Charge Coupled Device (CCD) chip. A 90° geometry between the incident radiation and the collecting system was employed. The entrance slit was set to 200 μm, while the slit between the premonochromator and the spectrograph was set to 3.5×10^4 μm. The 514.5 nm line of an Ar^+ laser (Coherent, model Innova 305) was used as the excitation radiation, providing *ca.* 60 mW at the sample position.

In order to overcome fluorescence, the spectra of guanine, cisplatin–guanine and the cisplatin–adenine adducts were obtained using a RFS 100/S Bruker Fourier transform Raman spectrometer, equipped with an InGaAs detector. The 1064 nm line provided by a Nd:YAG laser (Coherent, model Compass-1064/500N) was used as the incident radiation, yielding *ca.* 300 mW at the sample position. The resolution was set at 2 cm^{-1} and a 180° geometry was employed.

All experiments were run at room temperature and the samples (solids) were sealed in Kimax glass capillary tubes of 0.8 mm inner diameter.

INS. The INS intensity of each vibrational transition is normally expressed in terms of the so-called dynamic structure factor $S_i^*(Q,\nu_k)$, which has the simplified expression, for a given atom

$$S_i^*(Q,\nu_k) = \frac{(Q^2 u_i^2)}{3}\exp\left(-\frac{Q^2\alpha_i^2}{3}\right) \quad (1)$$

where Q ($Å^{-1}$) is the momentum transferred to the sample, ν_k is the energy of a vibrational mode, u_i (Å) is the displacement vector of atom i in mode k, σ is the neutron scattering cross section of the atom, and α_i (Å) is related to a mass-weighted sum of the displacements of the atom in all the vibrational modes. The harmonic frequencies (energies) of the vibrational modes correspond to eigenvalues, and the displacements to eigenvectors, of the dynamical matrix calculated by the Density Functional Theory – Plane-Wave (DFT-PW) methodology.

The spectra were obtained at the ISIS Pulsed Neutron Source of the Rutherford Appleton Laboratory (United Kingdom), on the TOSCA spectrometer.[43] This is an indirect geometry time-of-flight, high resolution ($\Delta E/E$) *ca.* 1.25%), broad range spectrometer. The samples (2–3 g) were wrapped in 4 × 4 cm aluminium foil sachets, which filled the beam, and placed in thin walled aluminium cans. To reduce the impact of the Debye–Waller factor (the exponential term in eqn (1)) on the observed spectral intensity, the samples were cooled to *ca.* 10 K. Data were recorded in the energy range −24 to 4000 cm^{-1} and converted to the conventional scattering law, $S(Q, \nu)$ *vs.* energy transfer (in cm^{-1}) through standard programs.

Simultaneous INS and Raman. The simultaneous INS and Raman experiments were carried out at the ISIS using the TOSCA spectrometer for collecting the INS data and a Renishaw inVia apparatus with a 300 mW 785 nm Toptica diode laser for obtaining the Raman spectra. In this configuration, the laser is fibre-optically coupled to a specially designed centrestick suitable for insertion into a 100 mm-bore cryostat, and is focused down to a spot size of *ca.* 50 μm diameter through a 1 mm thick sapphire window sited in the lid of the sample can,[44] yielding *ca.* 18 mW at the sample position The WIRE™ 2.0 software from Renishaw was used for focusing the laser onto the sample (by vertical tuning) and for acquiring the Raman data (the Raman signal returning along the same path).

The temperature at the sample was measured (with an accuracy of ±0.5 K) using calibrated rhodium–iron resistance thermometers attached to both the cryostat heat exchanger and the sample can.

EXAFS

X-ray absorption experiments were performed at the B18 beamline of the Diamond Light Source.[45] The measurements were carried out using the Cr-coated branch of collimating and focusing mirrors and a Si(111) double-crystal monochromator. The size of the beam at the sample position was approximately 1 mm (h) × 0.5 mm (v). All the samples were measured both in the solid state and in aqueous solution, into specific sample holders for liquids with 1 cm thickness. The solid samples were prepared as self-supported pellets using cellulose powder as the blank, the thickness was optimized to obtain an edge jump close to one and the pellets were measured inside a liquid nitrogen cryostat at a temperature of about 77 K. The data were

Table 1 Selected calculated and experimental geometric parameters[a] for the metal coordination sphere of the cDDP–G_2 adduct

	Calculated		
Parameter	Isolated molecule[c]	Solid[d]	Experimental[b]
Bond lengths (pm)			
Pt–N_7(I)	205.0	199.1	196.2
Pt–N_7(II)	205.0	202.2	201.0
Pt–NH_3(I)	206.5	203.7	204.8
Pt–NH_3(II)	206.5	203.4	196.9
Intracomplex distances (pm)			
N_7(I)–N_7(II)	298.6	295.8	383.1
O_6(I)–O_6(II)	461.0	310.0	410.2
Bond angles (degrees)			
NH_3–Pt–NH_3	92.39	93.92	93.21
N_7(I)–Pt–N_7(II)	93.49	94.99	90.87
N_7(I)–Pt–NH_3(I)	86.94	87.15	88.06
N_7(II)–Pt–NH_3(II)	86.94	85.24	87.79
N_7(I)–Pt–NH_3(II)	176.30	172.54	178.36
N_7(II)–Pt–NH_3(I)	176.30	169.91	177.09
Dihedral angles (degrees)			
NH_3(II)–Pt–C_5C_6(I)	11.73	2.52	9.25
NH_3(I)–Pt–C_5C_6(II)	−11.73	−36.87	−17.27

[a] Atoms are numbered according to Fig. 1. [b] From ref. 40. [c] At the DFT/mPW1PW level. [d] At the DFT-PW/LDA level.

 This journal is © the Owner Societies 2015

Published on 13 January 2015. Downloaded by Universidade de Coimbra on 06/02/2015 10:42:20.

measured in transmission, with ion chambers before and after the sample was filled with appropriate mixtures of inert gases to optimize the sensitivity (I_0: 80 mbar of Ar and 920 mbar of He, resulting in an overall efficiency of 15%; I_t: 250 mbar of Kr and 750 mbar of He, with 60% efficiency). The XAS data were collected in quick EXAFS mode, by scanning continuously the monochromator, each acquisition lasting about 6 minutes with several repetitions run for each sample in order to reach a good signal to noise ratio (10 to 30, depending on the concentration of Pt). The EXAFS spectra at the Pt L3-edge (11 564 eV) were obtained from 200 eV before the edge up to 1500 eV after the edge (corresponding to 20 $Å^{-1}$ in *k*-space), with a constant step size equivalent to 1 eV. EXAFS data on the solutions were collected in fluorescence mode, by means of a 9-element solid state Germanium detector and shortening the range to 1250 eV after the edge (corresponding to 18 $Å^{-1}$ in *k*-space) because of the lower signal to noise ratio. Data were normalized using the program Athena[46] with a linear pre-edge and polynomial post-edge background subtracted from the raw $\ln(I_t/I_0)$ data.

Theoretical calculations

Geometry optimization and optical vibrational spectra simulation. The quantum mechanical calculations were performed for the cisplatin adducts under study using the GAUSSIAN program[47] within the Density Functional Theory (DFT) approach, in order to properly account for the electron correlation effects. The hybrid mPW1PW91 exchange–correlation functional, which comprises a modified version of the exchange term of Perdew–Wang and the Perdew–Wang 91 gradient-corrected correlation functional,[48,49] was used, along with the double-zeta split valence basis set 6-31G**[50] for all atoms except platinum, for which the Los Alamos relativistic effective core potentials developed by Hay and Wadt[51] in a double-zeta splitting scheme (LANL2DZ), were applied, $n = 5$ and $n = 6$ being considered as valence electron shells.

Table 2 Main experimental and calculated vibrational wavenumbers for the cDDP–A_2 and cDDP–G_2 adducts

cDDP–A_2				cDDP–G_2					
Calculated	Experimental			Calculated		Experimental			
Isolated molecule[b]	FTIR	Raman	INS	Isolated molecule[b]	Solid[c]	FTIR	Raman	INS	Approximate description[a]
3364		3270		3476	3395	3442	3427	—	$\nu_{as}(NH_3)$
3318				3270	3286	3334	3295	—	$\nu_{as}(NH_2)$
3179		3191		3179	3187	3182	3219		$\nu(C_8H)$
					3140	3115	3147	—	$\nu_s(NH_2)$
3001		2960		2965	2875	2915	2942		$\nu(N_1H)$
2992		2927							$\nu_{as}(NH_3)$
3097		2880							$\nu(C_2H)$
				1721	1692	1697	1686	1678	$\nu(C{=}O)$
				1647	1637	1673		1629	$\alpha(NH_2) + \delta(N_9H)$
1597	1603	1577	1600	1600	1606	1631	1600	1589	$\delta_{as}(NH_3)$
				1497	1503	1475	1493	1474	$\nu(N_1C_2) + \nu(N_7C_8)$
1467	1470		1496						$\alpha(NH_2) + \delta(C_2H)$
1413		1455	—						$\delta(C_2H) + \delta(N_9H)$
1380	1385	1393	1375						$\nu(C_4C_5)$
1373	1353	1352	1348	1337	1399	1383	1387	1395	$\delta_s(NH_3)$
1328		1319	1308						$\delta(C_2H)$
1303	1312								$\nu(N_7C_5) + \delta(C_2H)$
1225	1230	1181	1225	1273	1260	1261	1256	1263	$\nu(N_9C_8)$
1133		1145		1168	1168	1175	1159	1266	$\delta(N_9H) + \delta(C_8H) + \nu(N_1C_6)$
1090	1116	1123	1126	1109	1112	1120	—	1114	$\delta(C_5N_9C_8) + \delta(C_6C_5N_9) + t(NH_2)$
				1046	1049	1043	1046	1050	$\delta(NH_2) + \delta(N_1H)$
1030	1040	1047	1014						$\tau(NH_2)$
932	947	944	955	923	943	949	—	913	$\rho(NH_3)$
				873	844	878	—	864	$\rho(NH_3)$
866	899	892	887						$\omega(NH_2)$
823	830	818		823	840	849	842	852	$\rho(NH_3)$
				688	680	688	679	677	$t(NH_2)$
705	723	720	735	623	645	644	645	635	$\gamma(C_8H)$ + ring breathing
655	643		616						$\gamma(N_9H)$
552	571		560	554	539		538	557	$\nu_s(NH_3{-}Pt{-}NH_3)$; $\tau(NH_2)$
536	538	516	540	547	523	503	515		$\nu_{as}(NH_3{-}Pt{-}NH_3)$
525		465							$\delta(N_1C_6N_6)$; $\delta(N_3C_4N_9)$
				375	370	—	373	374	$\delta(C_6{=}O)$; $t(N_7PtN_7)$
360	—	356							$\delta(N_7PtN_7)$; $\delta(C_5C_6N_6)$
309	—	312	324	267	273	—	278	274	$\delta(NH_3{-}Pt{-}NH_3)$
293	—	286		285	235	—		234	$\tau(NH_3)$
220	—	246	244						Adenine butterfly
152	—	161							$\gamma(N_7PtN_7)$

[a] Atoms are numbered according to Fig. 1. ν – stretching, δ – in-plane deformation, γ – out-of-plane deformation, α – scissoring, t – twisting, ρ – rocking, ω – wagging, τ – torsion, s – symmetric, as – anti-symmetric. [b] At the DFT/mPW1PW91 level, scaled as described in the Experimental section using scaling factors from ref. 22 and 53. [c] At the DFT-PW/LDA level, unscaled.

Published on 13 January 2015. Downloaded by Universidade de Coimbra on 06/02/2015 10:42:20.

Molecular geometries were fully optimized by the Berny algorithm, using redundant internal coordinates:[52] the bond lengths to within *ca.* 0.1 pm and the bond angles to within *ca.* 0.1°. The final root-mean-square (rms) gradients were always less than 3×10^{-4} hartree bohr^{-1} or hartree radian^{-1}. Harmonic vibrational wavenumbers, as well as Raman activities and infrared intensities, were obtained at the same theory level as the geometry optimizations.

In order to correct for anharmonicity, the calculated frequencies for the isolated molecules were scaled before comparing with the experimental data. Different scaling factors were applied to distinct frequency sets: adapted from Merrick and co-workers[53] for the organic moieties of the adducts (0.9513 and 0.9846 below and above 700 cm^{-1}, respectively); and the parameters developed by Amado *et al.*[22] for the inorganic part (H_3N–Pt–NH_3) (0.92 (ν_{NH_3}), 0.97 (δ_{NH_3}), 1.01 (ρ_{NH_3}) and 1.12 (ν_{PtN}, δ_{NPtN})). This was considered a valid approach since the vibrational transition energies of the adenine and guanine ligands are well separated from those involving the metal (*i.e.* there is no significant overlap between the vibrational eigenvectors of the organic and inorganic moieties of the adducts).

DFT Plane-Wave (DFT-PW) calculations were also performed for the systems under study, within the Perdew–Zunger local density approximation (LDA),[54] and using plane-wave expansions, as implemented in the PWSCF code from the Quantum Espresso package.[55] The atomic coordinates were fully optimized using the published crystal structures of anhydrous guanine and adenine as a starting point.[56,57] PW calculations performed for the cDDP–G_2 adduct were accomplished using the crystal structure of *cis*-[$Pt(NH_3)_2EG_2$]$SO_4 \cdot 4H_2O$ (EG = ethylguanine).[40] Unit cell parameters were kept at their experimental values. The ethyl groups in the asymmetric unit were deleted and the spatial coordinates of hydrogen atoms were inferred empirically and inserted in the crystal structure using the XCrysden software.[58] The pseudopotentials employed were of the norm-conserving type – a Von Barth–Car approach was applied to the H and C atoms,[59] a Martins–Troullier[60] type was used for O and N, and a Bachelet–Hamann–Schlüter[61] type for S. For Pt, a plane-wave-based norm-conserving relativistic pseudopotential was built,[26] to be applied with the Perdew–Zunger LDA functional. This choice of methods was guided by the fact that Raman activities can only be calculated with PWSCF methods, using a LDA DFT approach and norm-conserving pseudopotentials. A cut-off energy of 70 Ry and a Monkhorst–Pack grid[62] of $3 \times 3 \times 3$ were found to be sufficient to attain convergence. The dynamical matrix was calculated for the optimized geometries within the Density Functional Perturbation theory,[63] and was diagonalized to obtain the vibrational normal mode wavenumbers, as well as the Raman activities. No scaling was used for the wavenumbers calculated for the condensed phase.

Calculation of the INS spectra. The theoretical INS transition intensities were obtained from the calculated normal mode eigenvectors of the quantum mechanical calculations, and the spectra simulated using the dedicated aCLIMAX program.[64]

Calculation of EXAFS data. The fit of the experimental EXAFS data was performed by using the program Artemis, which is based on the FEFF code[65] for theoretical calculation of the scattering paths' intensities and phases contributing to the EXAFS signal.

Results and discussion

Optimized structures for the cisplatin–purine adducts

The calculated geometry for the most stable conformation of the cDDP–G_2 adduct is presented in Fig. 1, both for the isolated molecule and the condensed phase. Almost all crystal structures of cDDP–guanine adducts published so far have an HT (head-to-tail) orientation, with a preferred Pt coordination at the N_7 position of the purine ligand. However, since an HT arrangement in native DNA is unfavoured due to steric effects, the presently obtained solid state structure was based on the reported X-ray data for the HH (head-to-head) analogous system with ethylguanine,[40] including eight water molecules and two sulphate ions in the unit cell (due to cisplatin's activation with Ag_2SO_4). It is worth noticing that the two guanine ligands are not geometrically equivalent in this optimized geometry (I and II, Fig. 1(B)), as opposed to the isolated molecule (Fig. 1(A)).

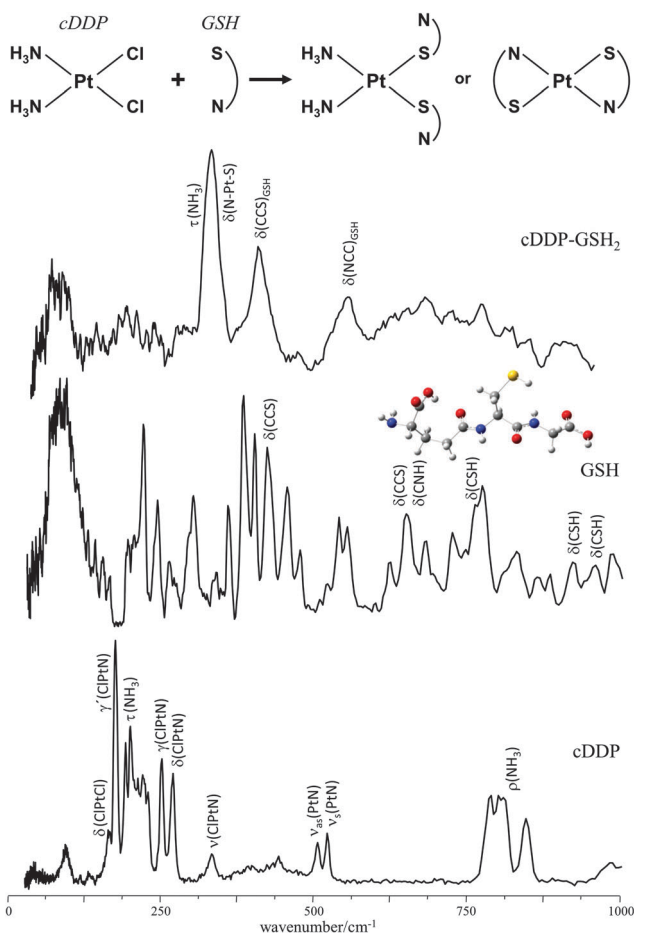

Fig. 2 INS experimental spectra for cisplatin (cDDP), reduced glutathione (GSH) and cDDP–GSH_2. The calculated structure (DFT/B3LYP 6-31G**) of reduced glutathione is also shown, as well as a schematic representation of some possible coordination modes to cisplatin (adapted from ref. 11).

 This journal is © the Owner Societies 2015

Published on 13 January 2015. Downloaded by Universidade de Coimbra on 06/02/2015 10:42:20.

The average Pt–N_7 bond length was calculated to be 201 pm for the solid (205 pm in the isolated molecule), in good agreement with the reported experimental values of 199 pm and 205 (respectively from X-ray crystallography[40,66,67] and NMR[68]). A quite strong H-bonding type interaction occurs between the carbonyl-oxygen from the base (O_6) and the drug NH_3, with a $d((N)H\cdots O_6)$ equal to 191.3 and 178.9 pm. The optimized geometric parameters presently obtained for the Pt(II) coordination sphere within the guanine adduct are given in Table 1, and compared with the reported X-ray diffraction values.[40]

Contrary to the cisplatin–guanine adduct, information on cDDP–A_2 is surprisingly scarce in the literature, despite the utmost importance of understanding the drug's preference for guanine over adenine for a successful rational design of new cisplatin-like antitumoural agents. Hence, no condensed phase calculations could be performed for this system due to lack of a suitable X-ray model. The optimized structure for the isolated molecule is shown in Fig. 1(A), displaying two equivalent adenine moieties as previously found for isolated cDDP–G_2, and a non-planar NH_2 group partly due to steric repulsion between the amine hydrogens and those of the drug NH_3 ligands ($d(N_6\cdots H(N)_{drug}$ = 202 pm)). Regarding the metal coordination site, the calculated Pt–NH_3 and Pt–N_7 bond lengths are fairly similar (208.0 and 204.8 pm, respectively) and just slightly longer than those obtained for cDDP–G_2 (206.5 and 205.0 pm, respectively, Table 1). Interestingly, when comparing both adducts the Pt–NH_3 bond length is the one displaying a more significant change, and not Pt–N_7 as could be expected.

Vibrational spectroscopy

The complementary INS, Raman and FTIR data gathered for the systems under study (Table 2) allowed us to detect and accurately assign their entire vibrational profile, including the low energy oscillators reflecting the metal coordination to

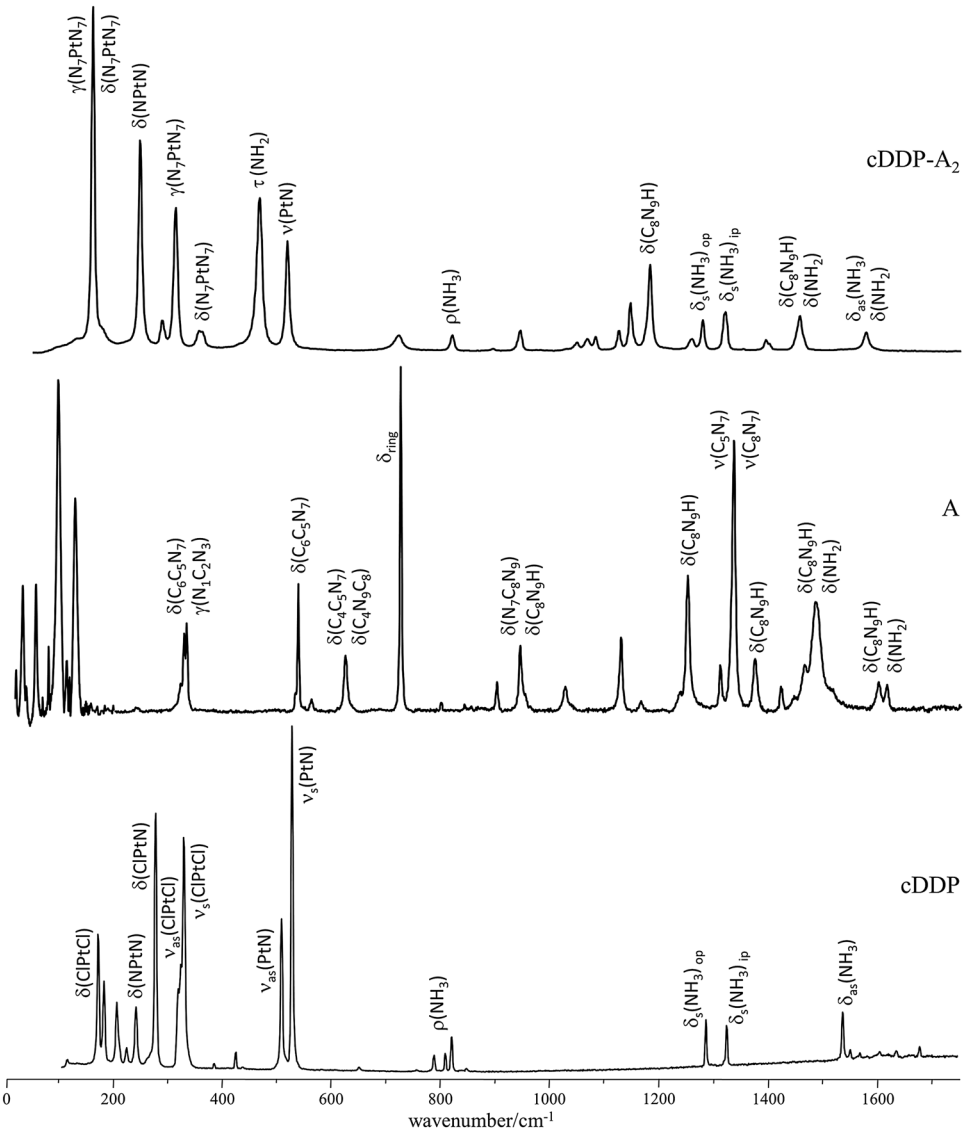

Fig. 3 Raman experimental spectra for cisplatin (cDDP), adenine (A,[28]) and cDDP–A_2.

Published on 13 January 2015. Downloaded by Universidade de Coimbra on 06/02/2015 10:42:20.

either N or S atoms, which is paramount for determining the exact coordination pattern of the drug to DNA. These results were interpreted in the light of the full conformational analysis previously performed by the authors for cisplatin[21–23,25,26] and the purine bases adenine[28] and guanine,[27] as well as for the optimized structures presently obtained for reduced glutathione (Fig. 2), [cDDP–A_2] and [cDDP–G_2] (Fig. 1).

The cisplatin–purine adducts exist as a fluxional mixture of conformers, as free rotation around the Pt–N_7 bond allows an equilibrium between the HH and HT atropisomers,[69] leading to a high degree of conformational freedom. This is responsible for the broadened features observed in the corresponding optical vibrational spectra, as well as for the complexity of the measured INS pattern. Additionally, the Raman intensities are considerably lower for the adducts than for the free bases (Fig. 3 and 4), which can be explained by the stacking of the purine molecules in the crystal lattice of the adduct, that lead to a decrease in polarisability. As expected, the intense Raman bands at 162 and 324 cm^{-1} ascribed to cisplatin's Cl–Pt–Cl deformation and Pt–Cl stretching modes, respectively,[25] are not detected for the adenine adduct (Fig. 3), showing that the sample is free from unreacted drug.

Indeed, the typical bands from the drug were found to disappear upon interaction with DNA bases, namely the Raman signals due to δ(ClPtCl) and ν(ClPtCl) (Fig. 3), and the INS features γ'(ClPtN), γ(ClPtN), δ(ClPtN) and ν_{as}(ClPtN) (Fig. 5 and 6), corresponding to the metal coordination environment in cisplatin. Additionally, new features, characteristic of drug binding to the DNA purines, were evident in the spectra of the adducts: For cDDP–A_2, $\delta(N_7PtN_7)$, δ(NCN) and $\delta(C_8H)$ were clearly observed in the Raman spectrum at 356, 465 and 1225 cm^{-1}, respectively, while the very intense Raman band at 1334 cm^{-1} assigned to adenine's $\nu(C_5N_7)$ and $\nu(C_8N_7)$ disappeared in the adduct (Fig. 3 and Table 2). Regarding cDDP–G_2, the $\gamma(N_7C_8N_9)$ and $\nu(C_5N_7)$ vibrations were detected in the Raman spectrum at 635 and 1046 cm^{-1}, and $\nu(PtN_7)$ and $\gamma(C_8N_9H)$ gave rise to INS bands at 557 and 1050 cm^{-1}. Guanine's (C_8N_9) and (C═O) stretching modes (at 1232/26, 1265/69, and 1549/1550 cm^{-1}, respectively, in Raman/INS[27]) were visibly affected by adduct formation, while guanine's INS signal from the butterfly mode was shifted from 177/196 to 274 cm^{-1} (Fig. 6 and Table 2). Formation of a stable drug–guanine entity was clearly evidenced by the shift detected in INS

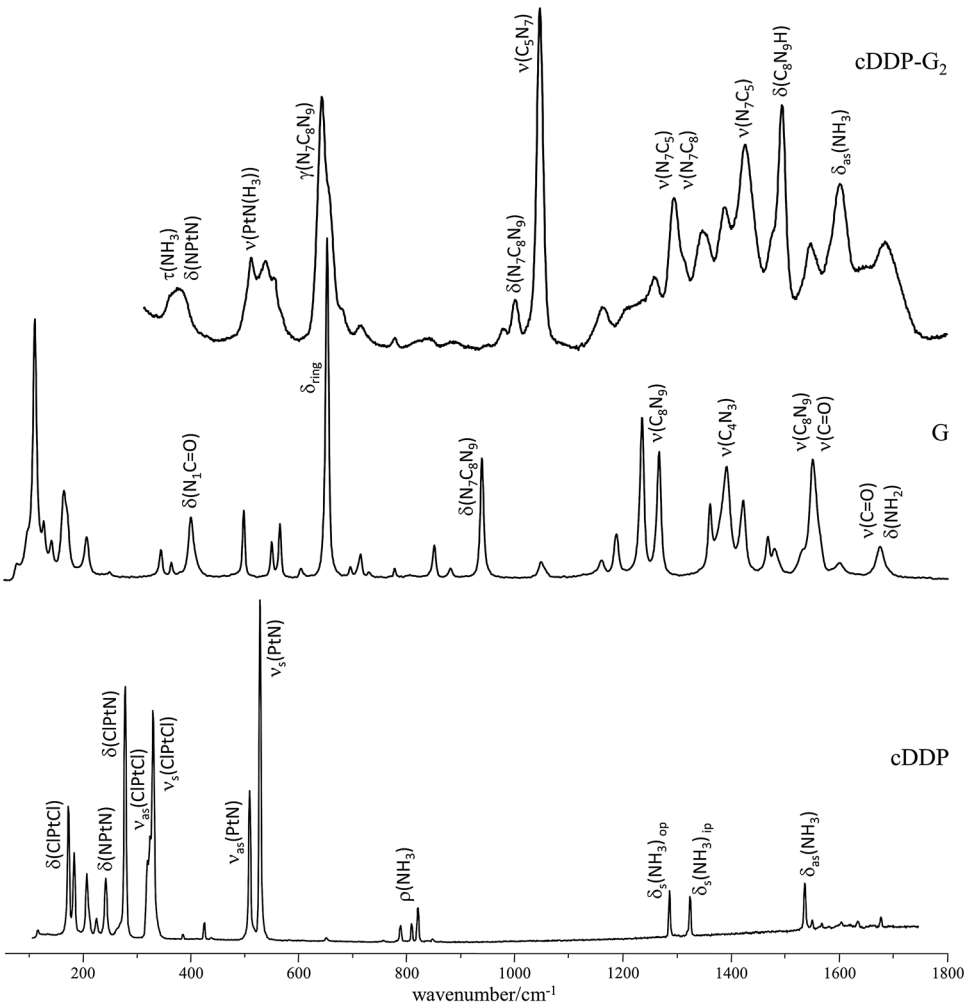

Fig. 4 Raman experimental spectra for cisplatin (cDDP), guanine (G,[27]) and cDDP–G_2.

 This journal is © the Owner Societies 2015

Published on 13 January 2015. Downloaded by Universidade de Coimbra on 06/02/2015 10:42:20.

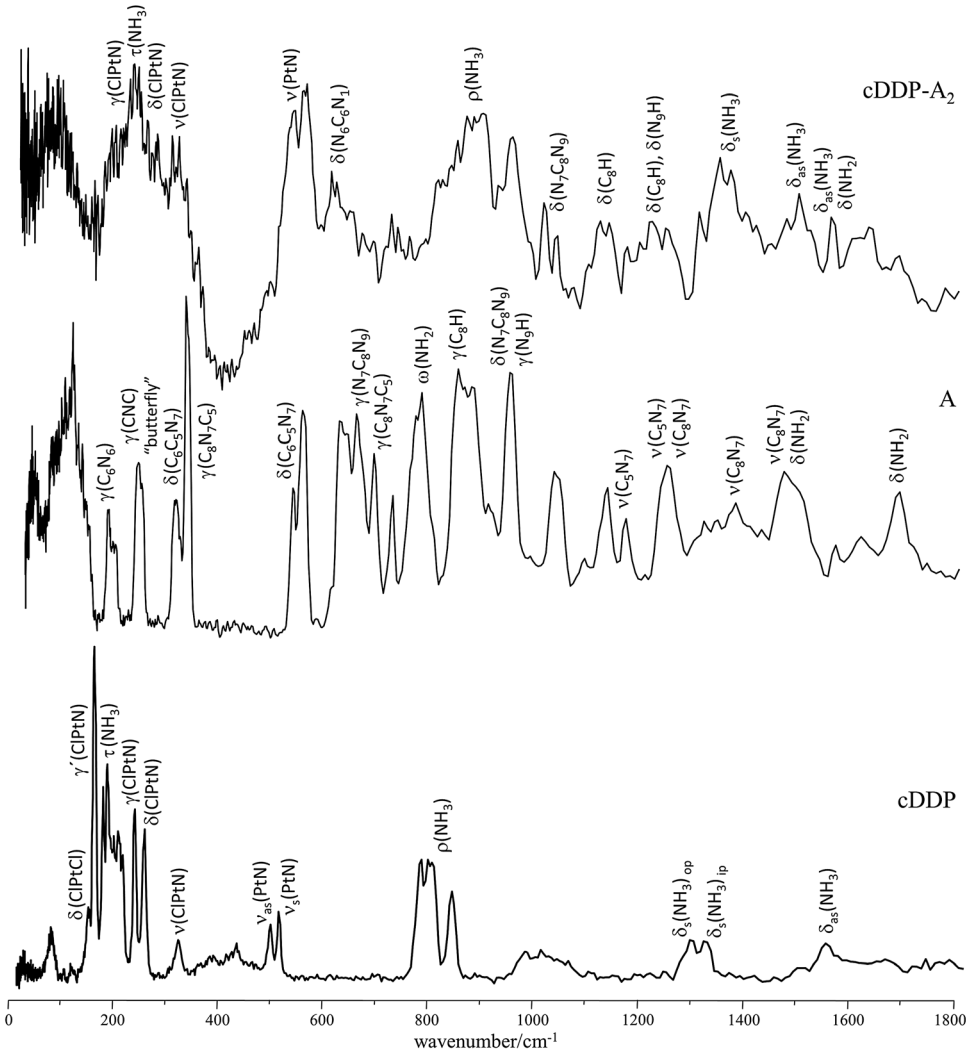

Fig. 5 INS experimental spectra for cisplatin (cDDP), adenine (A) and cDDP–A_2.

for the $\delta(N_1C_6{=}O)$ mode of the purine moiety in the adduct relative to the free base, from 403 in G[27] to 374 cm^{-1} in cDDP–G_2 (Fig. 6), due to a stabilizing H-bonding interaction between cisplatin's NH_3's and the carbonyl oxygen from the base. For both adducts, the INS $\rho(NH_3)$ and $\delta(NH_3)$ modes from the drug (at 808 and *ca.* 1300 cm^{-1}) were blue-shifted upon cDDP–purine coordination (to *ca.* 950/910 and 1350/1390 cm^{-1} for adenine and guanine adducts respectively, Fig. 5 and 6).

The conflicting nature of the studies reporting the formation of Pt–GSH adducts upon incubation of cisplatin with reduced glutathione,[9,11,70] (Fig. 2) and the involvement of this endogenous cellular antioxidant in cisplatin's acquired resistance mechanisms, urges a thorough understanding, at the molecular level, of cDDP–GSH interplay (*via* Pt binding to the thiol group, pk = 9.2[71]). This was presently tackled by simultaneous neutron and Raman scattering experiments that enabled us to collect complementary information under exactly the same conditions,[26,44] yielding most of the vibrational modes of the systems under study. Interaction with glutathione was detected in the spectral profiles of both GSH and the anticancer agent: the Raman ν(SH) mode from reduced (free) glutathione (at 2525 cm^{-1},[72] Fig. 7) was found to disappear (as expected) upon drug-binding, as well as most of the GSH very intense INS bands between 300 and 500 cm^{-1}, reflecting drug coordination (Fig. 2). Also, the carbonyl stretching modes from the amide and carboxylic GSH moieties (at 1628 and 1703 cm^{-1}) were strongly affected, and were hardly observed in the (cDDP–GSH) (1 : 2) adduct. Regarding cisplatin, low frequency bands typical of Pt–Cl coordination (both INS and Raman) disappeared as the chlorides were replaced by glutathione's sulfur atoms. New signals appeared such as those assigned to δ(N–Pt–S), at 334 cm^{-1}, while the bands due to ν(Pt–N), detected at 505/521 cm^{-1} for the free drug, were clearly affected by the presence of glutathione (Fig. 2). Apart from the intense band centred at 334 cm^{-1}, observed in both the Raman and INS spectra, two other distinctive features appear in the neutron scattering spectrum, at 410 and 555 cm^{-1}, ascribed to skeletal deformations within the glutathione molecule (δ(CCS) and δ(NCC), respectively), shifted relative to free GSH owing to metal coordination (Fig. 2). Additionally, glutathione coordination to Pt(II) is

Published on 13 January 2015. Downloaded by Universidade de Coimbra on 06/02/2015 10:42:20.

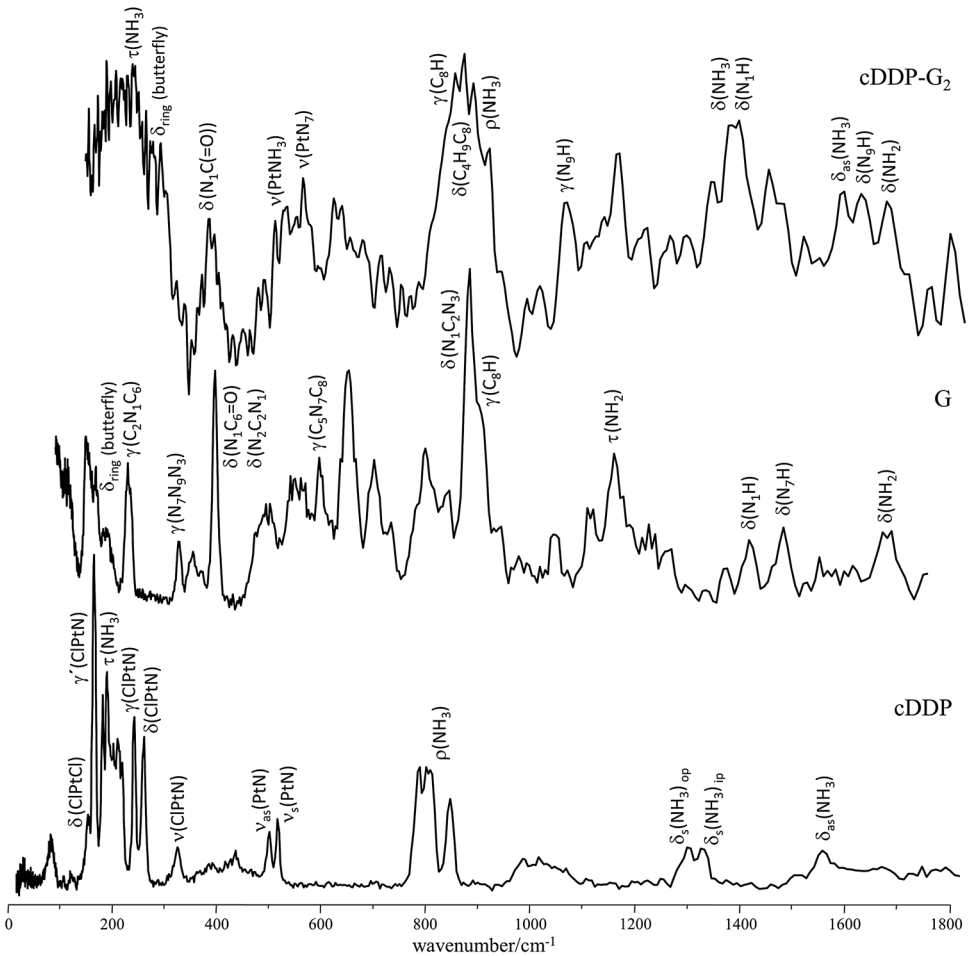

Fig. 6 INS experimental spectra for cisplatin (cDDP), guanine (G) and cDDP–G_2.

responsible for disruption of the $NH_3\cdots Cl$ intramolecular close contacts in cisplatin, leaving the ammine groups free to interact with the glutathione carbonyls *via* quite strong H-bonds, which explains the marked blue shift detected for $\tau(NH_3)$ in INS, from 200 cm^{-1} in the free drug[25] to *ca.* 330 cm^{-1} in cDDP$(GSH)_2$ (Fig. 2). These interactions also explain the blue shift detected for the drug's NH_3 rocking modes (INS bands centred at 800 cm^{-1})[19] upon GSH binding (Table 2). In the (1 : 2) cisplatin : glutathione adduct, the favoured binding mode is expected to be a monodentate one, through the preferred GSH's sulfur atoms, no NH_3 by S substitution taking place in the metal's coordination sphere (2S + 2N(H_3), Fig. 2), which is in accordance with the observed vibrational pattern, evidencing typical ν(Pt–S) features and shifted ν(Pt–N(H_3)) signals (probably to lower wavenumbers, *ca.* 350 cm^{-1}).

Although glutathione is recognized to play a major role in the mechanism of cellular resistance to cisplatin and cisplatin-like drugs, by effectively coordinating to Pt(II) before the drug reaches its target (DNA),[11,12,73] nothing is known (at the molecular level) regarding the role of GSH in promoting the disruption of platinated DNA adducts. The present simultaneous INS and Raman scattering data evidenced a clear difference between the spectra of cDDP–G_2 and that of the GSH-titrated adduct (cDDP–G_2 + GSH, Fig. 8), due to substitution of guanine (N_7) by glutathione (S atoms) in the metal coordination sphere. A very intense Raman band centred at around 330 cm^{-1} was a common feature to all GSH-containing samples (Fig. 7), assigned to ν(Pt–S) and not discernible by INS (due to the very low incoherent cross-section of sulfur). Still, attending to the detection of several characteristic INS bands from guanine – namely $\delta(N_1C_6{=}O)$ (at 376 cm^{-1}) and $\delta(C_4N_9C_8)$ (at 844 cm^{-1}) (Fig. 8) – GSH does not appear to substitute the purine base completely, both coexisting as Pt(II) ligands. This is corroborated by the EXAFS results for the drug–guanine adduct (see below) as opposed to the adenine homologue, and is justified by the higher stability of cDDP–G_2 relative to cDDP–A_2 (based on the formation of favouring $(N)H_{drug}\cdots O({=}C)_{guanine}H$-bonds).

EXAFS

Before performing a detailed fitting of the collected data, it is possible to get a sense of the local environment (first coordination sphere) of the Pt centre in the different samples by observing and comparing the different XAS signals. When analysing the cDDP solid state and aqueous solution it is clear that both XANES and EXAFS curves are almost identical, apart

 This journal is © the Owner Societies 2015

Published on 13 January 2015. Downloaded by Universidade de Coimbra on 06/02/2015 10:42:20.

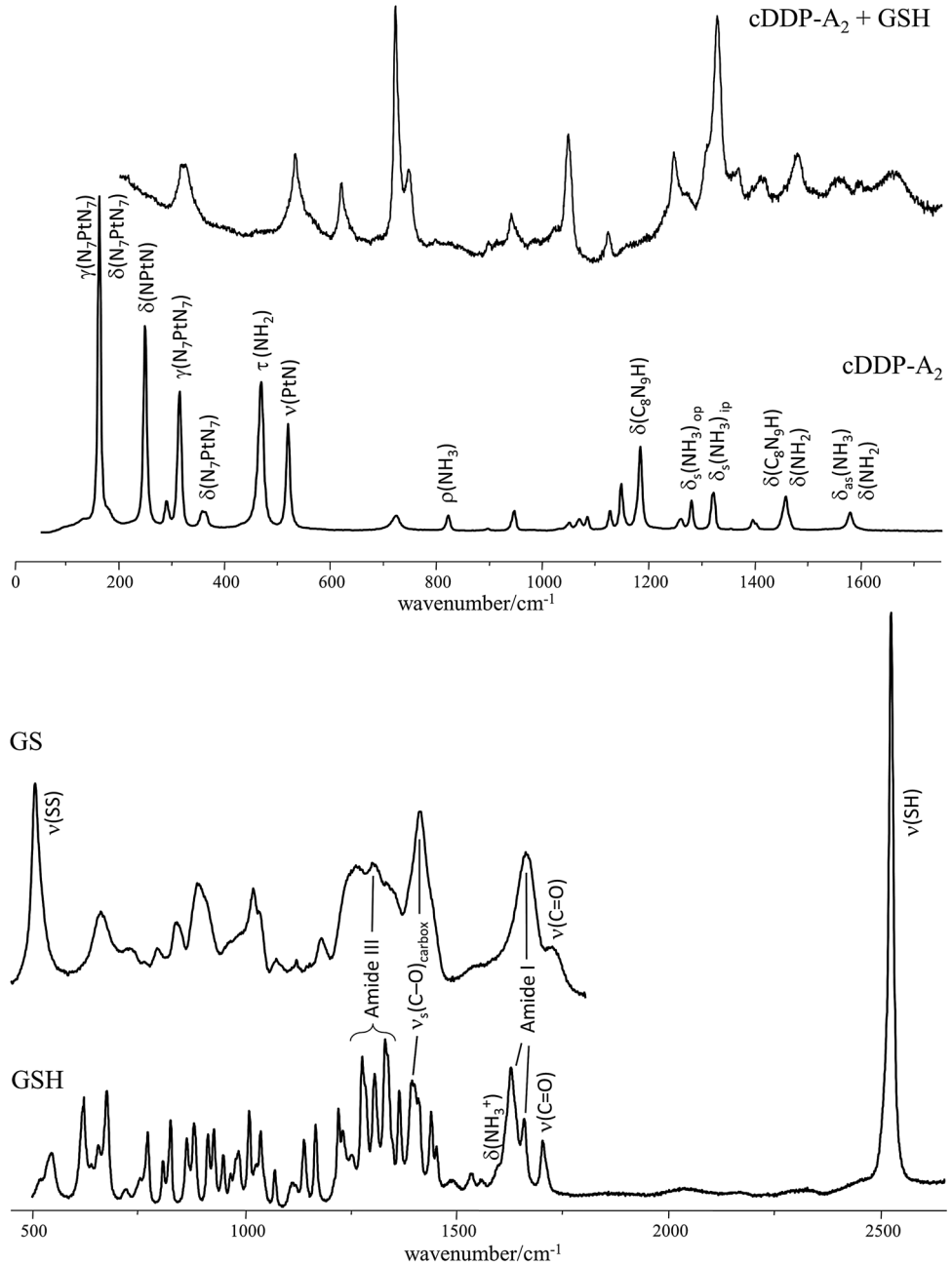

Fig. 7 Raman experimental spectra for reduced (GSH) and oxidised (GS) glutathione, for cDDP–A_2 and for cDDP–A_2 upon GSH titration (1 : 2).

from the fact that the data for aqueous solution are more noisy and from a slightly different intensity in the white line (that may be due to normalization procedures, or due to the fact that one measurement has been done in transmission and the other in fluorescence mode) (Fig. S1, ESI‡). In order to have a clear interpretation of the signals it is worth starting from the spectra of the references to obtain a deeper understanding of the signal obtained for all the other samples and disclose which kind of variations we could expect. Fig. 9 shows the XANES (a), EXAFS function (b) and Fourier transform (c) of $Pt(Cl)_4$, $Pt(NH_3)_4$ and $Pt(GSH)_4$ solid samples, which are our standards for Pt atoms with three different coordination shells (4 Cl, 4 N and 4 S atoms respectively). The figure shows how the position of the edge in the XANES does not shift conspicuously, and is almost the same for $Pt(NH_3)_4$ and $Pt(GSH)_4$. Hence it would be difficult to distinguish quantitatively between different ligands only on the basis of the XANES, although there are still appreciable changes in the features after the edge. On the other hand, the EXAFS shows a big difference in the Pt–N bond length in $Pt(NH_3)_4$ while it would be difficult to distinguish between Pt–Cl and Pt–S since they have comparable bond length and scattering power (due to the similar atomic number). The EXAFS fit of the standards (Table 3) allowed us to optimize the bond length and to obtain useful parameters such as amplitude (S_0^2), energy

Published on 13 January 2015. Downloaded by Universidade de Coimbra on 06/02/2015 10:42:20.

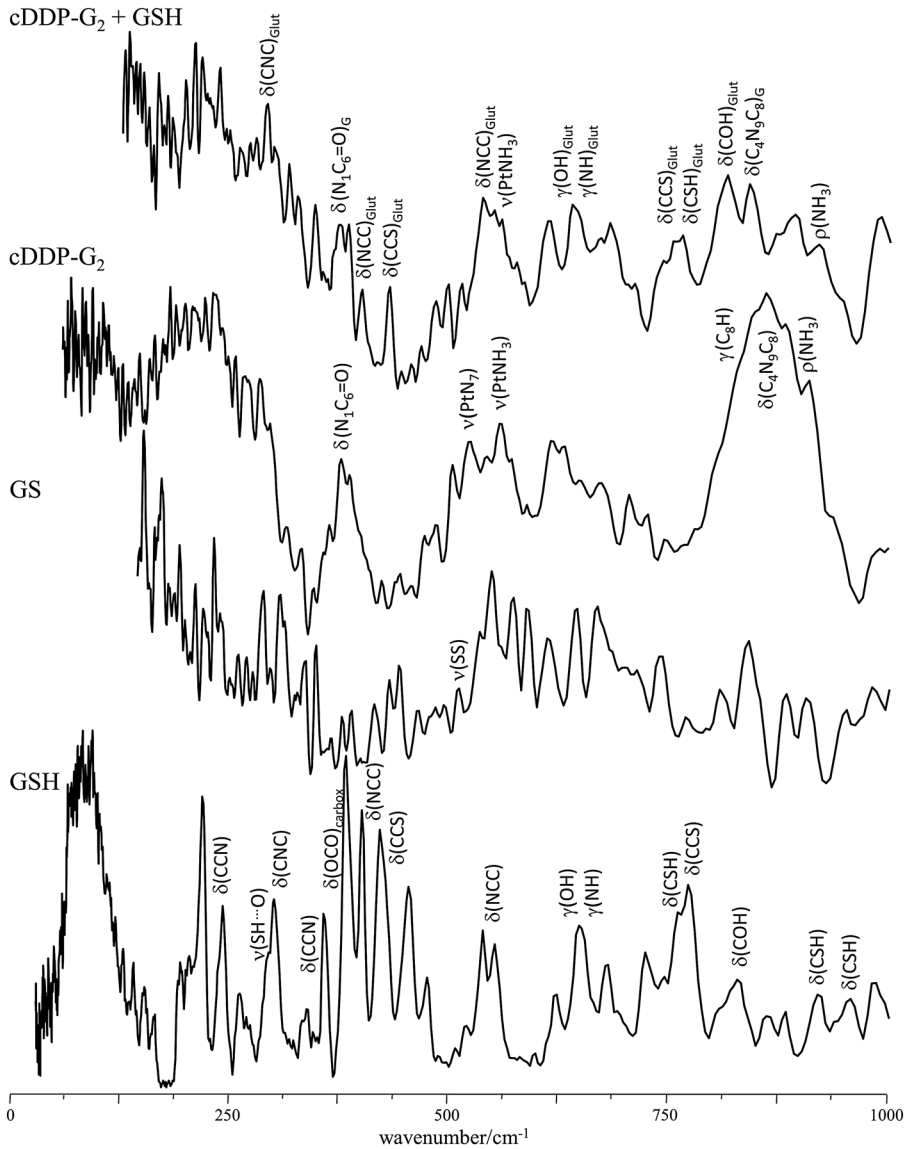

Fig. 8 INS experimental spectra for reduced (GSH) and oxidised (GS) glutathione, for cDDP–G_2 and for cDDP–G_2 upon GSH titration (1 : 2).

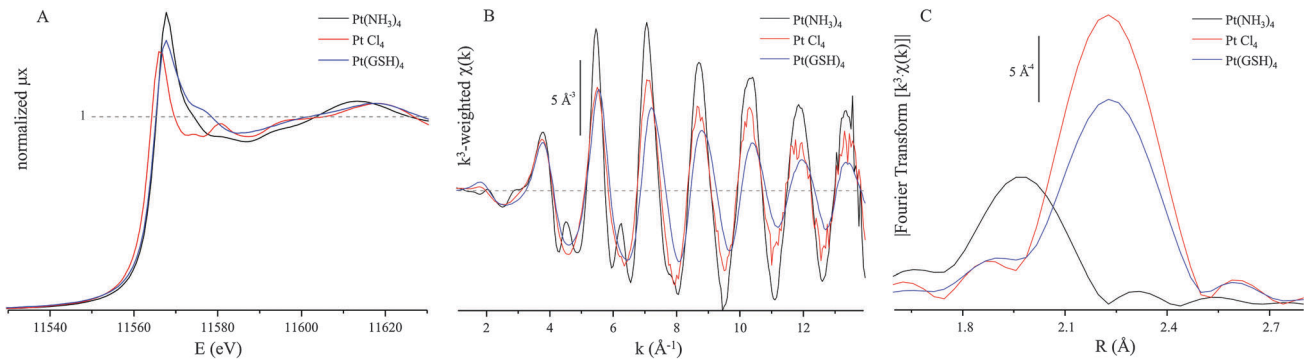

Fig. 9 (A) XANES, (B) EXAFS function $\chi(k)$ and (C) its Fourier transform for $Pt(NH_3)_4$, $Pt(Cl)_4$ and $Pt(GSH)_4$ standards, respectively, in black, red and blue lines.

 This journal is © the Owner Societies 2015

Published on 13 January 2015. Downloaded by Universidade de Coimbra on 06/02/2015 10:42:20.

Table 3 Results of EXAFS fit for standards[a]

Sample	*R*-factor	S_0^2	E_0 (eV)	CN	*R* (Å)	σ^2 (10^{-3} Å^2)
$Pt(NH_3)_4$	0.00931	0.88 ± 0.04	8.1 ± 0.6	4 N	2.039 ± 0.004	2.5 ± 0.4
$PtCl_4$	0.01158	0.73 ± 0.04	9.5 ± 0.7	4 Cl	2.309 ± 0.004	1.5 ± 0.4
$Pt(GSH)_4$	0.01981	0.81 ± 0.07	5.5 ± 0.8	4 S	2.313 ± 0.006	3.2 ± 0.7

[a] The fit was performed on the first shell of the EXAFS signal with coordination numbers fixed and all the other parameters free. S_0^2: passive electron reduction factor; CN: number and type of ligands bond to platinum; *R*: Pt–ligand distance; σ^2: Debye–Waller factor.

shift (E_0) and Debye–Waller factors (σ^2) that will be used as starting points for the two-phase fit of the samples where a mixed coordination is expected: *x*N ligands and (4 − *x*) Cl or S ligands.

Cisplatin–purine adducts

For cisplatin the number of first-neighbours around Pt(II) is 4 (2N/2Cl), in a square planar geometry. The number and type of neighbour atoms and their distance from the Pt(II) centre in the adducts under study were determined by analysis of the XANES and EXAFS spectra obtained for the (1 : 1) and (1 : 2) adenine and guanine adducts (Fig. 10) that reflected the coordination patterns PtN_3Cl for [cDDP–A] and [cDDP–G], and PtN_4 for [cDDP–A_2] and [cDDP–G_2]. A linear combination fit of the XANES data based on the two standards $Pt(NH_3)_4$ and $Pt(Cl)_4$ was used to estimate the percentage of N and Cl atoms in the Pt first coordination sphere. The results were 43% N and 57% Cl for cDDP (so approximately a coordination of PtN_2Cl_2) and 100% N ligands for [cDDP–A_2] and [cDDP–G_2] (so PtN_4). A more accurate EXAFS fit in the *R*-space of the first shell (1–2.5 Å) was performed, to double check the preliminary XANES results and obtain further information about the geometry such as bond length. For each spectrum, the fit was performed a first time leaving all the parameters free and a second time fixing the coordination number to the expected values (according to methods of synthesis, XANES estimation and optimized values from the first fit) to reduce the number of variables, correlations, and consequently errors relative to the other parameters optimized by the fit (see Table 4). It was found that the coordination numbers C.N. expected were confirmed to be 2 N and 2 Cl for cDDP and 4 N for [cDDP–A_2] and [cDDP–G_2]. It is worth noting that the Pt–N bond lengths were slightly shortened with respect to the $Pt(NH_3)_4$ reference, while the Pt–Cl bond lengths were slightly elongated. The high quality of the fits, appreciable in Fig. 10, was confirmed by the low values of the *R*-factor and by the fact that all the optimized values for the other parameters were in a reasonable range set by their physical meaning and were coherent with the ones found for the standards.

Cisplatin–glutathione adducts

The thiol-containing tripeptide glutathione (GSH) is an essential endogenous antioxidant that avoids severe oxidative damage to important cellular components, by acting as an electron donor (being converted into glutathione disulphide, GSSG). Although several reported studies have shown that GSH plays a major role in the mechanism of acquired cellular resistance to cisplatin and cisplatin-like drugs,[11,12] by coordinating to the drug's Pt(II) centre before this reaches its target (DNA), no molecular evidence exists on the role of glutathione in triggering disruption of platinated adenine or guanine adducts. Under physiological conditions glutathione is present in high concentrations in the cell (*ca.* 5 mM) and prompt disruption of the Pt–N bond in these DNA adducts can occur, GSH displacing the amine ligands from the purine bases and giving rise to the favoured Pt–S coordination.

In order to assess GSH competition for Pt(II) over DNA purine bases, cDDP–A_2 and cDDP–G_2 were titrated with reduced

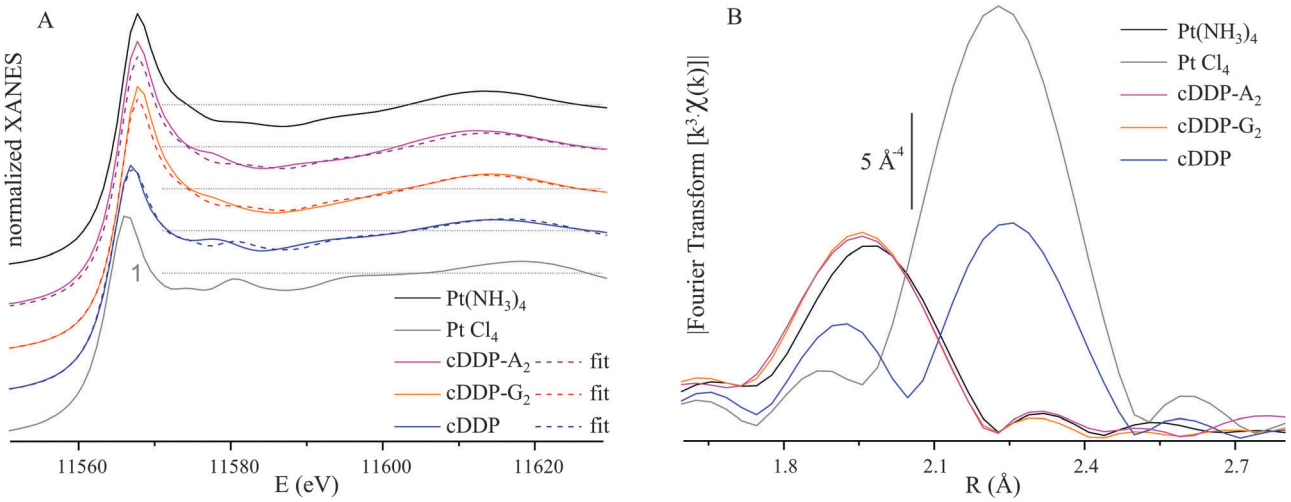

Fig. 10 (A) XANES, (B) Fourier transform of EXAFS $\chi(k)$ data and best fits for cisplatin and cisplatin–purine adduct samples.

Published on 13 January 2015. Downloaded by Universidade de Coimbra on 06/02/2015 10:42:20.

Table 4 Results of EXAFS fit for cisplatin and cisplatin–purine adducts[a]

Sample	*R*-factor	S_0^2	E_0 (eV)	CN_N	R_N (Å)	σ_N^2 (10^{-3} Å^2)	CN_{Cl}	R_{Cl} (Å)	σ_{Cl}^2 (10^{-3} Å^2)
cDDP	0.00871	0.82 ± 0.07	11.8 ± 1.1	2.3 ± 0.5	2.043 ± 0.019	2.8 ± 2.2	1.7 ± 0.5	2.317 ± 0.006	1.4 ± 1.0
	0.00935	0.79 ± 0.05	11.5 ± 0.7	2	2.036 ± 0.009	1.8 ± 0.8	2	2.315 ± 0.004	1.8 ± 0.4
cDDP–A_2	0.01164	0.92 ± 0.40	9.7 ± 1.4	4.0 ± 0.9	2.019 ± 0.018	2.5 ± 1.6	0.0 ± 0.9	—	—
	0.02789	0.91 ± 0.07	9.5 ± 0.8	4	2.019 ± 0.007	2.4 ± 0.9	0	—	—
cDDP–G_2	0.00805	0.81 ± 0.04	10.6 ± 1.3	4.0 ± 0.4	2.024 ± 0.007	1.8 ± 0.9	0.0 ± 0.4	—	—
	0.01940	0.80 ± 0.06	10.8 ± 0.8	4	2.023 ± 0.005	1.7 ± 0.5	0	—	—

[a] For each sample, the fit was performed on the first shell of the EXAFS signal with all parameters free (first row) and with coordination numbers fixed to expected values (second row). S_0^2: passive electron reduction factor; CN_X: number of X atoms bond to platinum; R_X: Pt–X distance; σ_X^2: X atom Debye–Waller factor.

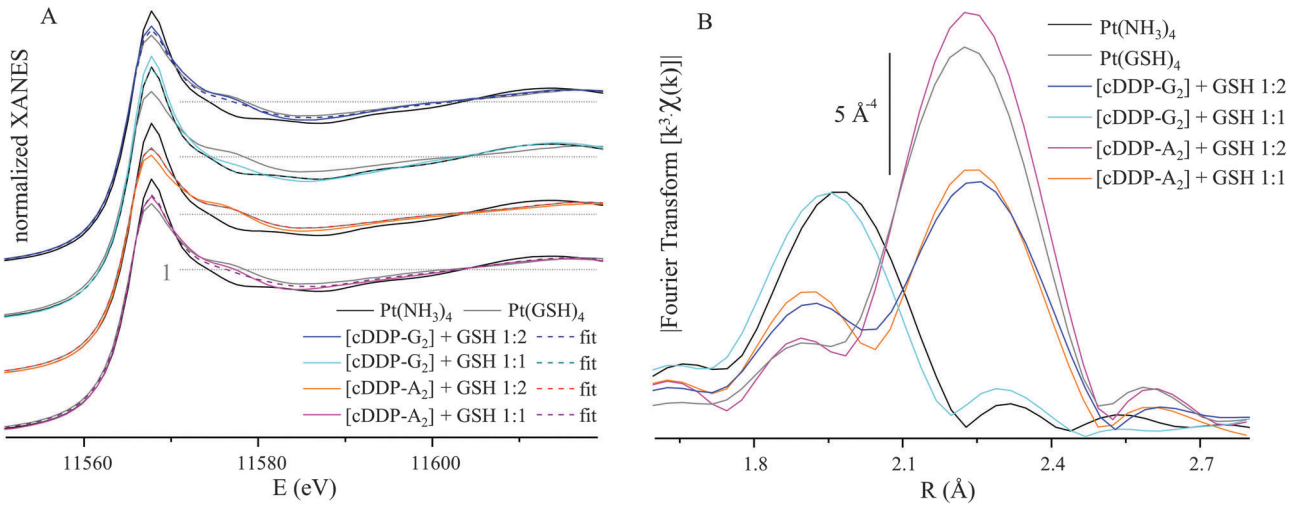

Fig. 11 (A) XANES and (B) Fourier transform of EXAFS $\chi(k)$ data and best fits for cisplatin–purine adducts with increasing GSH ratio ((1 : 1) and (1 : 2)).

glutathione (GSH) and the changes in the local atomic structure around Pt(II) relative to the DNA adducts were screened by EXAFS. The spectroscopic pattern of the resulting products, upon breaking of the adenine and guanine (1 : 2) adducts, revealed at least two sulfur atoms in the metal's first coordination sphere (Fig. 11), as proof of platinum's coordination to glutathione, either in a mono- or bidentate pattern, respectively, through its sulphur atoms alone or *via* both sulphur and nitrogen sites (Fig. 2). These data corroborate platinum's preference for sulfur as compared to nitrogen binding sites (from A or G) that led to a partial or complete Pt–N by Pt–S substitution in the metal's coordination sphere. This constitutes a clear spectroscopic evidence of the well-recognized resistance mechanism to cisplatin's cytotoxic activity *in vivo* due to glutathione competition.

Additionally, these results establish cisplatin's preference for guanine over adenine, due to the formation of a favoured H-bond between cisplatin's NH_3 and guanine's carbonyl oxygen (Fig. 1). Actually, upon titration with increasing amounts of glutathione a complete N for S substitution in the metal's coordination sphere was observed only for [cDDP–A_2] (PtN_4 to PtS_4 coordination sphere), while a N_2S_2 local environment around the metal was obtained for the titrated guanine species (PtN_4 to PtN_2S_2, Fig. 11).

As already done for the cisplatin–purine adducts, a linear combination fit of the XANES data was performed also for this series of samples using as standards $Pt(NH_3)_4$ and $Pt(GSH)_4$. Although the difference between the spectra of the standards is less evident, so a precise evaluation of each component's contribution is more complicated, it is still possible to estimate the percentage of N and S atoms in the Pt first coordination sphere. In sum, in the case of adenine a partial disruption of Pt–N bonds in favour of Pt–S (64%) is found for the (1 : 1) ratio and the full PtS_4 coordination is reached upon increasing the ratio of glutathione to (1 : 4). On the other hand, for guanine the (1 : 1) ratio does not show any interference by GSH and is comparable to PtN_4 coordination; while the (1 : 2) highlights a disruption which is not completed with 25% of N and 75% of S atoms. The EXAFS fit was performed using the same procedure already described for the cisplatin–purine adducts and the results are reported in Table 5. The large reported errors in two of the four fits are due to the fact that, to maintain a coherent method and have a better comparison of the results, these fits consider both Pt–N and Pt–S scattering paths even if only N (cDDP–A_2 + GSH 1 : 2) or only S (cDDP–G_2 + GSH 1 : 1) neighbours are expected. The introduction of three extra parameters that cannot be optimized in the fit procedure caused a higher overall uncertainty due to the correlations between variables. The fits were then refined (even rows in Table 5) using only one type of ligand (either N or S), fixing the coordination numbers to 4 and optimizing solely the amplitude S_0^2, which yielded errors

 This journal is © the Owner Societies 2015

Published on 13 January 2015. Downloaded by Universidade de Coimbra on 06/02/2015 10:42:20.

Table 5 Results of EXAFS fit for cisplatin–purine adducts with increasing GSH ratio 1 : 1 and 1 : 2[a]

Sample	*R*-factor	S_0^2	E_0 (eV)	CN_N	R_N (Å)	σ_N^2 (10^{-3} Å^2)	CN_S	R_S (Å)	σ_S^2 (10^{-3} Å^2)
cDDP–A_2 + GSH 1 : 1	0.01076	0.82 ± 0.08	10.0 ± 2.1	2.0 ± 0.8	2.039 ± 0.029	2.3 ± 2.8	2.0 ± 0.8	2.316 ± 0.010	1.7 ± 1.5
	0.01076	0.82 ± 0.05	10.0 ± 0.8	2	2.038 ± 0.012	2.2 ± 1.1	2	2.316 ± 0.005	1.7 ± 0.5
cDDP–A_2 + GSH 1 : 2	0.01414	0.81 ± 9.99	10.4 ± 1.1	0.0 ± 9.9	—	—	4.0 ± 9.9	2.321 ± 0.006	2.5 ± 0.6
	0.01414	0.80 ± 0.06	10.4 ± 0.7	0	—	—	4	2.321 ± 0.004	2.5 ± 0.5
cDDP–G_2 + GSH 1 : 1	0.01642	0.85 ± 9.99	10.4 ± 1.2	3.8 ± 9.9	2.023 ± 0.007	2.1 ± 0.7	0.2 ± 9.9	—	—
	0.01642	0.81 ± 0.05	10.4 ± 0.7	4	2.023 ± 0.005	2.1 ± 0.6	0	—	—
cDDP–G_2 + GSH 1 : 2	0.01214	0.93 ± 0.11	10.2 ± 2.9	2.1 ± 0.9	2.045 ± 0.044	3.8 ± 3.8	1.9 ± 0.9	2.306 ± 0.014	2.2 ± 1.8
	0.01245	0.92 ± 0.07	9.9 ± 0.9	2	2.035 ± 0.015	3.4 ± 1.9	2	2.318 ± 0.006	2.4 ± 0.7

[a] For each sample, the fit was performed on the first shell of the EXAFS signal with all parameters free (first row) and with coordination numbers fixed to expected values (second row). S_0^2: passive electron reduction factor; CN_X: number of X atoms bond to platinum; R_X: Pt–X distance; σ_X^2: X atom Debye–Waller factor.

of 0.05 that are comparable to those obtained for all the other samples. The optimized coordination numbers thus obtained confirmed the trends observed from the XANES linear combination studies, and led to 2 Pt–N and 2 Pt–S bonds for (1 : 2) [cDDP–A_2] + GSH and 4 Pt–S bonds for (1 : 4) [cDDP–A_2] + GSH, while PtN_2S_2 and PtN_4 coordination patterns were achieved for [cDDP–G_2] + GSH upon increase of the glutathione ratio. The coordination of GSH seems to introduce an elongation of the remaining Pt–N bonds with respect to the optimized distances of the cisplatin–purine adducts and a larger spread in the distribution of the distances evidenced by higher Debye–Waller factors. The high quality of the fits, appreciable in Fig. 11, was confirmed by the low values of the *R*-factor and by the fact that all the optimized values for the other parameters were coherent with the ones found for the standards.

Conclusions

The results obtained in this study of cisplatin's adducts with DNA purine bases, as well as with glutathione, has enabled a thorough understanding of the cisplatin–DNA interplay at the molecular level, which is the basis for the drug's growth-inhibitory and cytotoxic activities, as well as of the acquired resistance process due to intracellular drug scavenging by glutathione prior to reaching the biological target.

The complementary INS, FTIR and Raman data, combined with DFT-PW theoretical approaches, has allowed access to the complete vibrational pattern of the systems under study, including the low energy region reflecting the metal coordination sphere and leading to the identification of their vibrational spectral signature. EXAFS has led to an unambiguous determination of the local environment of the Pt(II) centre in the drug adducts with the purine bases A and G during interaction with the pharmacological target (pharmacodynamics), and yielded a precise molecular picture of their glutathione-induced metabolic deactivation (pharmacokinetics). Additionally, cisplatin's preference for guanine over adenine during interaction with DNA was evidenced by glutathione titration assays of the [drug–purine] adducts: upon GSH titration of [cDDP–A_2] and [cDDP–G_2] a complete N by S substitution in the metal's coordination sphere was only observed for the former, reflecting a somewhat weaker Pt–A binding relative to Pt–G, *i.e.* a higher stability of the guanine species. Additionally, the EXAFS experiments currently performed allowed unequivocal verification of Pt coordination to GSH.

Following the synthesis and cytotoxicity evaluation of this kind of metal-based antineoplastic agents, the combined use of EXAFS and vibrational spectroscopy techniques, coupled with theoretical calculations, has led to an improved understanding of the mode of action of these compounds, at the molecular level, and provided valuable clues for the rational design of novel cisplatin-like drugs, such as polynuclear Pt(II)- and Pd(II)-polyamine chelates which have been studied by the authors in the last few years. These are intended to display higher efficiency, lower toxicity, decreased acquired resistance and possibly allow oral administration.

Acknowledgements

The authors acknowledge financial support from the Portuguese Foundation for Science and Technology – PEst-OE/QUI/UI0070/2014. The Advanced Computing Laboratory of the University of Coimbra is also acknowledged for allotted computer time. The STFC Rutherford Appleton Laboratory is thanked for access to neutron beam facilities. The INS work was supported by the European Commission under the 7th Framework Programme through the Key Action: Strengthening the European Research Area, Research Infrastructures (Contract no.: CP-CSA_INFRA-2008-1.1.1 Number 226507-NMI3). Diamond Light Source is acknowledged for time on B18/Core EXAFS (proposal 8434), under the European Funding programme Calypso FP7.

References

1 B. Rosenberg, L. Van Camp and T. Krigas, *Nature*, 1965, **205**, 698–699.
2 B. Rosenberg, L. Van Camp, J. E. Trosko and V. H. Mansour, *Nature*, 1969, **222**, 385–386.
3 L. Kelland, *Nat. Rev. Cancer*, 2007, **7**, 573–584.
4 N. P. Farrell, *Curr. Top. Med. Chem.*, 2011, **11**, 2623–2631.
5 M. P. M. Marques, *ISRN Spectrosc.*, 2013, **2013**, 1–29.
6 S. E. Sherman and S. J. Lippard, *Chem. Rev.*, 1987, **87**, 1153–1181.

Published on 13 January 2015. Downloaded by Universidade de Coimbra on 06/02/2015 10:42:20.

7 J. Reedijk, *Proc. Natl. Acad. Sci. U. S. A.*, 2003, **100**, 3611–3616.
8 P. C. A. Bruijnincx and P. J. Sadler, *Curr. Opin. Chem. Biol.*, 2008, **12**, 197–206.
9 D. Hagrman, J. Goodisman and A. K. Souid, *J. Pharmacol. Exp. Ther.*, 2004, **308**, 658–666.
10 X. Wang and Z. Guo, *Anticancer Agents Med. Chem.*, 2007, **7**, 19–34.
11 Y. Kasherman, S. Sturup and D. Gibson, *J. Med. Chem.*, 2009, **52**, 4319–4328.
12 H. H. W. Chen and M. T. Kuo, *Met.-Based Drugs*, 2010, **2010**, 1–8.
13 E. Lipiec, W. Kwiatek, J. Czapla, B. Wood, J. Szlachetko, G. B. Deacon, Y. Kayser and J. Sá, *Dalton Trans.*, 2014, **43**, 13839–13844.
14 D. Bouvet, A. Michalowicz, S. Crauste-Manciet, D. Brossard and K. Provost, *Inorg. Chem.*, 2006, **45**, 3393–3398.
15 M. Obata, M. Harada, H. Ohi, S. Hirohara, M. Gottchaldt and S. Yano, *Chem. Pharm. Bull.*, 2009, **57**, 1107–1109.
16 K. Provost, D. Bouvet-Muller, S. Crauste-Manciet, J. Moscovici, L. Olivi, G. Vlaic and A. Michalowicz, *Biochimie*, 2009, **91**, 1301–1306.
17 C. Coulombeau, Z. Dhaouadi, M. Ghomi, H. Jobic and J. Tomkinson, *Eur. Biophys. J.*, 1991, **19**, 323–326.
18 Z. Dhaouadi, M. Ghomi, J. C. Austin, R. B. Girling, R. E. Hester, P. Mojzes, L. Chinsky, P. Y. Turpin and C. Coulombeau, *J. Phys. Chem.*, 1993, **97**, 1074–1084.
19 M. Shanmugasundaram and M. Puranik, *J. Raman Spectrosc.*, 2009, **40**, 1726–1748.
20 A. W. Parker, C. Y. Lin, M. W. George, M. Towrie and M. K. Kuimova, *J. Phys. Chem. B*, 2010, **114**, 3660–3667.
21 S. M. Fiuza, A. M. Amado, P. J. Oliveira, V. A. Sardão, L. A. E. Batista de Carvalho and M. P. M. Marques, *Lett. Drug Des. Discovery*, 2006, **3**, 149–151.
22 A. M. Amado, S. M. Fiuza, M. P. M. Marques and L. A. E. Batista de Carvalho, *J. Chem. Phys.*, 2007, **127**, 185104.
23 S. M. Fiuza, A. M. Amado, M. P. M. Marques and L. A. E. Batista de Carvalho, *J. Phys. Chem. A*, 2008, **112**, 3253–3259.
24 S. M. Fiuza, A. M. Amado, H. F. Santos, M. P. M. Marques and L. A. E. Batista de Carvalho, *Phys. Chem. Chem. Phys.*, 2010, **12**, 14309–14321.
25 L. A. E. Batista de Carvalho, M. P. M. Marques, C. Martin, S. F. Parker and J. Tomkinson, *ChemPhysChem*, 2011, **12**, 1334–1341.
26 M. P. M. Marques, R. Valero, S. F. Parker, J. Tomkinson and L. A. E. Batista de Carvalho, *J. Phys. Chem. B*, 2013, **117**, 6421–6429.
27 R. P. Lopes, M. P. M. Marques, R. Valero, J. Tomkinson and L. A. E. Batista de Carvalho, *Spectrosc. Int. J.*, 2012, **27**, 273–292.
28 R. P. Lopes, R. Valero, J. Tomkinson, M. P. M. Marques and L. A. E. Batista de Carvalho, *New J. Chem.*, 2013, **37**, 2691–2699.
29 M. P. M. Marques, M. T. Girão da Cruz, M. C. Pedroso de Lima, A. Gameiro, E. Pereira and P. Garcia, *Biochim. Biophys. Acta, Mol. Cell Res.*, 2002, **1589**, 63–70.
30 L. J. Teixeira, M. Seabra, E. Reis, M. T. Girão da Cruz, M. C. Pedroso de Lima, E. Pereira, M. A. Miranda and M. P. M. Marques, *J. Med. Chem.*, 2004, **47**, 2917–2925.
31 A. S. Soares, S. M. Fiuza, M. J. Gonçalves, L. A. E. Batista de Carvalho, M. P. M. Marques and A. M. Urbano, *Lett. Drug Des. Discovery*, 2007, **4**, 460–463.
32 R. Tummala, P. Diegelman, S. M. Fiuza, L. A. E. Batista de Carvalho, M. P. M. Marques, D. L. Kramer, K. Clark, S. Vujcic, C. W. Porter and L. Pendyala, *Oncol. Rep.*, 2010, **24**, 15–24.
33 I. F. Duarte, I. Lamego, J. Marques, M. P. M. Marques, B. J. Blaise and A. M. Gil, *J. Proteome Res.*, 2010, **9**, 5877–5886.
34 S. M. Fiuza, J. Holy, L. A. E. Batista de Carvalho and M. P. M. Marques, *Chem. Biol. Drug Des.*, 2011, **77**, 477–488.
35 T. M. Silva, S. Oredsson, L. Persson, P. Woster and M. P. M. Marques, *J. Inorg. Biochem.*, 2012, **108**, 1–7.
36 T. M. Silva, S. Oredsson, S. Kumar, M. P. M. Marques, L. Persson and S. Oredsson, *PLoS One*, 2013, **8**, e55651.
37 T. M. Silva, S. M. Fiuza, M. P. M. Marques, L. Persson and S. Oredsson, *Amino Acids (Biochemistry & Molecular Biology)*, 2014, **46**, 339–352.
38 B. Lippert, *Coord. Chem. Rev.*, 1999, **182**, 263–295.
39 B. Lippert and C. Raudaschl, *Inorg. Chim. Acta*, 1984, **93**, 43–50.
40 H. Schoellhorn, G. Raudaschl-Sieber, G. Mueller, U. Thewalt and B. Lippert, *J. Am. Chem. Soc.*, 1985, **107**, 5932–5937.
41 S. J. Berners-Price and P. W. Kuchel, *J. Inorg. Biochem.*, 1990, **38**, 305–326.
42 D. Gibson, Y. Kasherman, D. Kowarski and I. Freikman, *JBIC, J. Biol. Inorg. Chem.*, 2006, **11**, 179–188.
43 http://www.isis.stfc.ac.uk/instruments/tosca/tosca4715.html.
44 M. A. Adams, S. F. Parker, F. Fernández-Alonso, D. J. Cutler, C. Hodges and A. King, *Appl. Spectrosc.*, 2009, **63**, 727–732.
45 A. J. Dent, G. Cibin, S. Ramos, A. D. Smith, S. M. Scott, L. Varandas, M. R. Pearson, N. A. Krumpa, C. P. Jones and P. E. Robbins, *14th International Conference on X-Ray Absorption Fine Structure*, vol. 190, 2009.
46 B. Ravel and M. J. Newville, *J. Synchrotron Radiat.*, 2005, **12**, 537–541.
47 M. J. Frisch, *et al.*, *Gaussian 03, Revision D.01*, Gaussian, Inc, Wallingford, CT, 2004.
48 J. P. Perdew, K. Burke and Y. Wang, *Phys. Rev. B: Condens. Matter Mater. Phys.*, 1996, **54**, 16533–16539.
49 C. Adamo and V. Barone, *J. Chem. Phys.*, 1998, **108**, 664–675.
50 G. A. Petersson, A. Bennett, T. G. Tensfeldt, M. A. Allaham, W. A. Shirley and J. Mantzaris, *J. Chem. Phys.*, 1988, **89**, 2193–2218.
51 P. J. Hay and W. R. Wadt, *J. Chem. Phys.*, 1985, **82**, 270–283.
52 C. Peng, P. Y. Ayala, H. B. Schlegel and M. J. Frisch, *J. Comput. Chem.*, 1996, **17**, 49–56.
53 J. P. Merrick, D. Moran and L. Radom, *J. Phys. Chem.*, 2007, **111**, 11683–11700.
54 J. P. Perdew and A. Zunger, *Phys. Rev. B: Condens. Matter Mater. Phys.*, 1981, **23**, 5048–5079.
55 P. Giannozzi, N. Bonini, M. Calandra, R. Car, C. Cavazzoni, D. Ceresoli, G. L. Chiarotti, M. Cococcioni, I. Dabo,

 This journal is © the Owner Societies 2015

Published on 13 January 2015. Downloaded by Universidade de Coimbra on 06/02/2015 10:42:20.

A. Stefano de Gironcoli, S. Fabris, G. Fratesi, R. Gebauer, U. Gerstmann, C. Gougoussis, A. Kokalj and M. Lazzeri, *J. Phys.: Condens. Matter*, 2009, **21**, 1–19.
56 K. Guille and W. Clegg, *Acta Crystallogr., Sect. C: Cryst. Struct. Commun.*, 2006, **62**, o515–o517.
57 R. J. Fram, *Curr. Opin. Oncol.*, 1992, **4**, 1073–1079.
58 A. Kokalj, *J. Mol. Graphics Modell.*, 1999, **17**, 176–179.
59 A. del Corso, S. Baroni, R. Resta and S. de Gironcoli, *Phys. Rev. B: Condens. Matter Mater. Phys.*, 1993, **47**, 3588–3592.
60 N. Troullier and J. L. Martins, *Phys. Rev. B: Condens. Matter Mater. Phys.*, 1991, **43**, 1993–2006.
61 G. B. Bachelet, D. R. Hamann and M. Schlüter, *Phys. Rev. B: Condens. Matter Mater. Phys.*, 1982, **26**, 4199–4228.
62 H. J. Monkhorst and J. D. Pack, *Phys. Rev. B: Solid State*, 1976, **13**, 5188–5192.
63 P. Gianozzi and S. Baroni, in *Handbook of Materials Modeling, Vol. 1: Methods and Models*, ed. S. Yip, E. Kaxiras, N. Marzari and B. Trout, Springer, 2005.
64 A. J. Ramirez-Cuesta, *Comput. Phys. Commun.*, 2004, **157**, 226–238.
65 J. J. Rehr, S. I. Zabinsky and R. C. Albers, *Phys. Rev. Lett.*, 1992, **69**, 3397–3400.
66 F. Coste, J. M. Malinge, L. Serre, M. Leng and C. Zelwer, *Nucleic Acids Res.*, 1999, **27**, 1837–1846.
67 P. M. Takahara, C. A. Frederick and S. J. Lippard, *J. Am. Chem. Soc.*, 1996, **118**, 12309–12321.
68 A. Gelasco and S. J. Lippard, *Biochemistry*, 1998, **37**, 9230–9239.
69 S. O. Ano, F. P. Intini, G. Natile and L. G. Marzilli, *Inorg. Chem.*, 1999, **38**, 2989–2999.
70 T. Shoeib and B. L. Sharp, *Inorg. Chim. Acta*, 2013, **405**, 258–264.
71 T. N. Huckerby, A. J. Tudor and J. G. Dawber, *J. Chem. Soc., Perkin Trans.*, 1985, 759–770.
72 M. Picquart, L. Grajcar, M. H. Baron and Z. Abedinzadeh, *Biospectroscopy*, 1999, **5**, 328–337.
73 B. Stordal and M. Davey, *Life*, 2007, **59**, 696–699.